MNRAS **000**, 000–000 (0000) Preprint 27 March 2017 Compiled using MNRAS LATEX style file v3.0

The Immitigable Nature of Assembly Bias: the Impact of Halo Definition on Environmental Effects

Antonio S. Villarreal,[1⋆] Andrew R. Zentner,[1†] Yao-Yuan Mao,[1‡] Christopher W. Purcell,[2§] Andrew P. Hearin,[3¶] Frank C. van den Bosch,[3‖] and Benedikt Diemer[4⋆⋆]

[1] *Department of Physics and Astronomy & Pittsburgh Particle Physics, Astrophysics, and Cosmology Center (Pitt-PACC), University of Pittsburgh, Pittsburgh, PA*
[2] *Department of Physics and Astronomy, West Virginia University, Morgantown, WV*
[3] *Department of Astronomy, Yale University, Hew Haven, CT*
[4] *Center for Astrophysics, Harvard University, Cambridge, MA*

27 March 2017

ABSTRACT

Recent work has shown the importance of environment to the properties of dark matter halos. This brings conflict to standard implementations of the halo model and excursion set theory which assume that the properties of a population within the halo is determined by the mass of the halo alone. We seek to find a definition of the size of a halo that allows us to minimize the impact of assembly bias on halo model calculations. We analyze the dependence on environment of our properties using the method of marked correlation functions for several different halo definitions, utilizing the Diemer & Kravtsov (2015) simulations. We find that the strength of assembly bias has a strong dependence on the measured halo mass, even when using marks normalized around fixed mass. We note that differences in halo definition, sample selection, and properties of interest can greatly impact the measurement of assembly bias, potentially explaining conflicting results in the literature. These results suggest that halo assembly bias appears increasingly difficult to resolve using the definitions common in current halo finder techniques, possibly pointing toward the necessity of methods such as utilizing the halo splashback radius.

Key words: cosmology: dark matter – cosmology: large-scale structure of Universe – galaxies: formation –galaxies: halos – methods: numerical

1 INTRODUCTION

In the concordance cosmology, galaxies and clusters form within dark matter halos (e.g., White & Rees 1978; Blumenthal et al. 1984; Mo et al. 2010). Numerical simulations have provided a solid understanding of the abundances, properties, and clustering of dark matter halos in the standard cosmological model. Accordingly, it is possible to compute the clustering statistics of galaxies given a model for the relationship between galaxies and dark matter halos. Such halo occupation models have been used to interpret large-scale structure measurements and constrain models of galaxy evolution (Yang et al. 2003; Tinker et al. 2005; Zehavi et al. 2005; Porciani & Norberg 2006; van den Bosch et al. 2007; Zheng et al. 2007; Conroy & Wechsler 2009; Yang et al. 2009; Zehavi et al. 2011; Guo et al. 2011; Wake et al. 2011; Yang et al. 2011, 2012; Leauthaud et al. 2012; Rodríguez-Puebla et al. 2012; Behroozi et al. 2013b; Moster et al. 2013; Tinker et al. 2013; Cacciato et al. 2013; More et al. 2013; Guo et al. 2014; Zu & Mandelbaum 2015). To date, the vast majority of halo occupation models rely on a key assumption, namely that the probability of a halo to host a number of galaxies of a particular type depends only upon

⋆ E-mail: asv13@pitt.edu
† E-mail: zentner@pitt.edu
‡ E-mail: yymao@pitt.edu
§ E-mail: cwpurcell@mail.wvu.edu
¶ E-mail: andrew.hearin@yale.edu
‖ E-mail: frank.vandenbosch@yale.edu
⋆⋆ E-mail: benedikt.diemer@cfa.harvard.edu

halo mass. It is now well known that the clustering strength of halos depends upon properties such as halo formation time (Gao et al. 2005; Harker et al. 2006; Wechsler et al. 2006; Gao & White 2007; Croton et al. 2007; Zentner 2007; Dalal et al. 2008; Li et al. 2008; Lacerna & Padilla 2011), concentration (Wechsler et al. 2006; Faltenbacher & White 2010; Mao et al. 2015), and other halo properties (Bett et al. 2007; Hahn et al. 2007a,b; Faltenbacher & White 2010; van Daalen et al. 2012; Fisher & Faltenbacher 2016; Sunayama et al. 2016; Chaves-Montero et al. 2016). If galaxy properties depend upon these halo properties, a phenomenon known as galaxy *assembly bias*, then standard halo occupation modeling will fail (Zentner et al. 2014) and more complex models (Gil-Marín et al. 2011; Hearin et al. 2016b) are necessary.

In this work, we explore the possibility of simplifying halo occupation modeling, at least for some applications, by altering the definition of a halo. Though motivated broadly by spherical collapse **[ARZ: Cite the classic spherical collapse papers here, such as Lacey & Cole 1993 and so on.]**, specific halo definitions have become a matter of convention that vary considerably in the literature. Many authors define halos using a friends-of-friend (FoF) algorithm applied to the particle distribution **[ARZ: Cite the famous Davis, Efstathiou, Frenk, and White paper from the 1980s]**. More often, authors define halos by spherical overdensity (SO) regions within which the mean density exceeds a particular threshold. The threshold used varies significantly. With respect to the mean density of the universe, commonly used thresholds are 178, 180, 200, and ∼340 times the mean background density, the last of these being the "virial" overdensity in a concordance ΛCDM universe. Significantly higher values of the overdensity parameter are often used in studies of X-ray emission from cluster-sized halos.

Our work is an attempt to exploit halo definition to work for the convenience of the practitioner. We study the strength of various halo assembly bias signals as a function of halo definition. This is motivated, in large part, by recent literature that suggests that a large portion of assembly bias stems from halos in the relatively dense environments surrounding larger halos (Wang et al. 2007; Warnick et al. 2008; More et al. 2015; Sunayama et al. 2016). Moreover, the environmental impacts of halos on one another has been shown to extend beyond well beyond traditional virial radii. (Adhikari et al. 2014; Diemer & Kravtsov 2014; Wetzel et al. 2014; More et al. 2015; Wetzel & Nagai 2015) Halos in dense environments (e.g., near other large halos) exhibit anomalous properties (e.g., formation times, concentrations, etc.) compared to field halos in part because of their interactions with their larger, neighbor halos. It seems interesting to ask whether or not a halo definition in which large halos contain many of these smaller, anomalous neighbor halos, thus using the halo concept to draw a more meaningful boundary around regions within which highly nonlinear effects are important, can mitigate halo assembly bias. Assessing this strategy is the aim of our paper.

We restrict ourselves to halos that are defined by spherical regions and we study the strength of halo assembly bias as a function of the density threshold used to demarcate these halos. We find that for halo properties that measure the degree of central mass concentration, there exist halo definitions in which assembly bias may be greatly mitigated. However, the definitions which mitigate concentration-based assembly bias are mass dependent; high-mass, cluster-sized halos appear to have little assembly bias for a traditional overdensity definition of $\Delta \approx 200$, while low-mass halos ($\sim 10^{11}\,h^{-1}\mathrm{M}_{\odot}$) require $\Delta \approx 20$. Any mitigation strategy must be complex and mass dependent, as might be expected given the mass dependence of the assembly bias effect Wechsler et al. (2006). We find that we cannot mitigate the assembly bias of halos selected by properties other than concentration, such as halo spin, halo shape, and number of satellite halos. These results suggest that any mitigation scheme will likely be quite complex if it all practical. **[ARZ: I plan to add something here after I complete my run through the paper.]**

In § 2 of this paper, we discuss the cosmological simulations and halo finders utilized in the analysis. In § 3, we discuss and define the halo properties used as our tracers of assembly bias. In § 4, we discuss the statistics that we use to measure environmental effects after halo redefinition. We also discuss our method of removing known mass scaling from halo properties. In § 5, we present our findings and consider how the change of halo definition impacts measures of assembly bias. In § 7, we discuss the significance of our results in the context of halo modelling. We also consider the nature of assembly bias as a function of halo definition.

2 SIMULATIONS AND HALO IDENTIFICATION

In order to study the effects of halo redefinition, we use three cosmological N-body simulations of structure formation. The Diemer & Kravtsov (2015) simulations each utilize a Planck best-fit cosmology with $\Omega_{\mathrm{M}} = 0.32$, $\Omega_{\Lambda} = 0.68$, and $h_0 = 0.67$. We use three simulation boxes with comoving sizes of 125, 250, and 500 h^{-1}Mpc respectively. The particle masses are 1.6×10^8, 1.3×10^9, and 1.0×10^{10} $h^{-1}\mathrm{M}_{\odot}$ respectively, implying a total of 1024^3 particles in each simulation. The three simulations have force softening scales of 2.4, 5.8, and 14 h^{-1}kpc . We refer to each simulation as L0125, L0250, or L0500 for the remainder of the paper. This set of simulations allows us to probe the resolution effects inherent in halo finding (due to the varying resolutions of the simulations) and to probe the mass dependence of halo clustering over a wider range of halo masses than would be possible with only one simulation from the set. For example, L0125, with its higher resolution, contains the least massive resolved halos, while L0500 has the most robust statistics for the most massive halos as a result of the larger simulation volume.

To identify halos, we use the `ROCKSTAR` halo finder, which works on the phase space algorithm described in Behroozi, Wechsler & Wu (2013a). In short, `ROCKSTAR` determines initial groupings of particles using a Friends-of-Friends algorithm in phase space before applying the spherical overdensity halo definition in order to determine halo properties of interest. Unbound particles are removed prior to the calculation of halo mass and other halo properties. Our method of halo redefinition is to change how halo size is calculated as part of the `ROCKSTAR` pipeline. A halo is given a radius, r_{Δ}, determined by

$$\bar{\rho}(r_{\Delta}) = \Delta \rho_{\mathrm{m}}, \tag{1}$$

where the mean density within a spherical volume of radius r is $\bar{\rho}(r)$, Δ is the overdensity parameter, and $\rho_{\rm m}$ is the mean background mass density of the simulation. The resulting halo size calculation can have a large variation depending on the choice of Δ. The number chosen for Δ varies throughout the literature from $\Delta \approx 178$ to $\Delta \approx 340$ or higher for X-ray studies of clusters. We choose to vary the size of a halo by treating the overdensity parameter as tunable, expanding the range from $\Delta = 340$ to $\Delta = 20$. While this range is greater than the differences between most the common overdensity choices, this broad range enables a fairly extensive exploration of environmental effects on halo properties as a function of halo definition[1]. **[ARZ: I think that for completeness, you have to quote the linking length parameters that you used so that somebody else can test your methods if they want to. Please add this.]**[ASV: Added to the footnote.]

An additional benefit of the ROCKSTAR software is the ability to identify substructure, commonly referred to in the literature as subhalos. Effectively, all density peaks are identified within the simulation and if a halo exists within the phase space of another halo, the less massive of the two is defined to be a subhalo of the more massive companion. The more massive companion is referred to as the host halo. This process continues until all halos identified in the simulation have been designated as either host halos or subhalos.

3 HALO PROPERTIES

As has long been well known, halo mass is the property that most strongly affects halo clustering. In this paper, we aim to study the strength of halo clustering as a function of halo properties other than mass. We will refer to these properties as "auxiliary" halo properties in this paper. The properties we study are described in this section.

3.1 Measures of Halo Concentration

We investigate the clustering of halos as a function of a number of halo properties that have been shown to influence halo clustering at fixed halo mass. We explore two definitions of halo concentration. The first stems from a fit of the spherically-averaged halo density profile, $\rho(r)$, to a Navarro et al. (1997); hereafter, NFW density profile,

$$\rho(r) = \frac{\rho_0}{\frac{r}{r_{\rm s}}(1+\frac{r}{r_{\rm s}})^2}, \quad (2)$$

where the density scale, ρ_0, and the scale radius, $r_{\rm s}$, are parameters that are fit to the density profile of each halo. The standard definition of halo concentration is then

$$c_{\rm NFW} = \frac{r_\Delta}{r_{\rm s}}, \quad (3)$$

where r_Δ is the radius of the halo given an overdensity parameter, Δ, defining the halo and $r_{\rm s}$ is the inferred halo scale radius. We use the NFW concentrations computed by the ROCKSTAR halo finder, which are derived from a fit to the halo density profile.

The NFW concentration defined in the previous paragraph has the shortcoming that it depends upon a parametric description of dark matter halos, so we study the clustering dependence of halos as a function of a non-parametric description of halo concentration as well. In particular, we use the "velocity-ratio" concentration,

$$c_{\rm V} = \frac{V_{\rm max}}{V_\Delta}, \quad (4)$$

where $V_{\rm max}$ is the maximum circular velocity achieved within the halo and V_Δ is the circular velocity at the halo radius, r_Δ. All halos of the same mass have the same value of V_Δ; however, they exhibit a variety of $V_{\rm max}$ values depending upon the degree to which their masses are concentrated toward the halo center. The quantity $c_{\rm V}$ is a non-parametric measure of halo concentration and can be measured from simulation snapshots without fitting halo density profiles. Consequently, $c_{\rm V}$ is robust to halo density profile parameterizations and halo profile fitting procedures.

Halo concentrations are interesting to investigate for these purposes for a number of reasons. First of all, the environment dependence of halo concentrations is known to be strong for standard halo definitions. Second, halo concentrations are of interest in the modeling of galaxy clustering and gravitational lensing statistics (and their cross correlations). In the case of galaxy clustering, the relevance is indirect, because galaxies may not trace the mass densities of their host halos. In the case of gravitational lensing, the mass distribution is the primary quantity of interest and halo concentrations are directly related to predictions for lensing statistics. Third, concentrations can be measured from individual simulation snapshots easily and halo concentrations are known to be strongly correlated with the formation histories of dark matter halos with earlier forming halos having higher concentrations at fixed halo mass (Wechsler et al. 2002; Zhao et al. 2003; Wechsler et al. 2006; Zhao et al. 2009). As such, exploring the concentration dependence of halo clustering may yield insight into the age dependence of halo clustering without the need for constructing merger trees. This is particularly important in the present study in which the halo finding is performed repeatedly for many different values of Δ. Constructing a self-consistent merger tree from which halo formation history can be studied requires halo finding at all simulation snapshots for each new value of Δ, which is a computationally prohibitive task.

In the present paper, we limit our study to halo properties that can be measured from a single simulation snapshot. However, halo formation histories correlate with halo concentrations with significant scatter and this correlation may depend upon environment, so the reader should be wary of drawing conclusions about the environmental dependence of halo formation by extrapolating our results on halo concentration. We will explore measures of halo age directly in a forthcoming follow-up study dedicated to halo formation histories.

Figure 1 shows the mean $c_{\rm NFW}$-M_Δ relation for halos defined with $\Delta = 200$ in L0125, L0250, and L0500. For each simulation, we consider halos only above a minimum mass threshold to ensure that property measurements are

[1] It is worth noting that the ROCKSTAR linking length parameter must be adjusted as Δ varies in order to ensure that SO halos contain all relevant particles. The value we choose ($0.4\ h^{-1}$Mpc) is large enough that it works for all definitions, but is poorly optimized for speed.

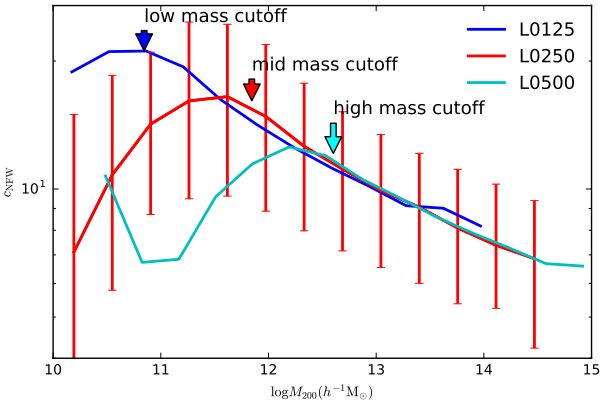

Figure 1. The relationship between the NFW concentration and halo mass for each of our simulations with $\Delta = 200$. In order of increasing simulation volume, the blue line corresponds to the concentration-mass relation from simulation L0125, the red line corresponds to L0250, and the cyan line corresponds to L0500. The red error bars show the 68% spread in parameter values within that mass bin for L0250. These errors are comparable to those of the other simulations within the region of interest. Each simulation is subject to resolution limitations at different halo masses. We show with arrows the minimum M_{200} mass thresholds that we adopt in our analyses using the same color code as the concentration-mass relations, going from L0125 to L0500 from left to right. Note the deviation from a monotonic trend as a result of resolution effects.

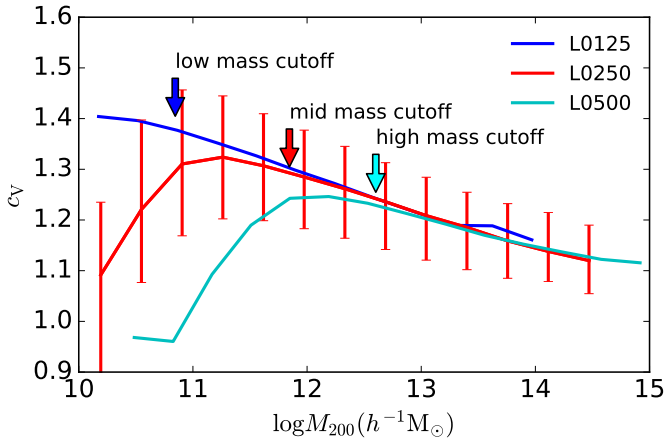

Figure 2. The relationship between the velocity ratio concentration and halo mass for each of our simulations with $\Delta = 200$. In order of increasing simulation volume, the blue line corresponds to the concentration-mass relation from simulation L0125, the red line corresponds to L0250, and the cyan line corresponds to L0500. The red error bars show the 68% spread in parameter values within that mass bin for L0250. These errors are comparable to those of the other simulations within the region of interest. Each simulation is subject to resolution limitations at different halo masses. We show with arrows the minimum M_{200} mass thresholds that we adopt in our analyses using the same color code as the concentration-mass relations, going from L0125 to L0500 from left to right. Note the deviation from a monotonic trend as a result of resolution effects.

not compromised by resolution effects. The minimum mass thresholds are shown as the vertical lines in Fig. 1 and listed in Table 1. Similar to Fig. 1, Figure 2 shows the relation between the velocity-ratio concentration, $c_{\rm V}$, and halo mass. In the interest of completeness, Figure 3 shows the relationship between $c_{\rm NFW}$ and $c_{\rm V}$ on a halo-by-halo basis. As is evident, the two concentration proxies are strongly correlated and exhibit a $\sim 6\%$ scatter indicating that $c_{\rm NFW}$ and $c_{\rm V}$ indeed encode similar information about each halo.

3.2 Halo Shape

In addition to halo concentrations, we examine halo clustering as a function of a variety of other halo properties. We study halo clustering as a function of halo shape, s, quantified by the ratio of the halo minor, c and major axis, a, lengths,

$$s = \frac{c}{a}. \tag{5}$$

The halo shapes we used were measured with `ROCKSTAR` by calculating the mass distribution tensor,

$$M_{ij} = \frac{1}{N}\sum_{N} x_i x_j, \tag{6}$$

for all particles within the halo radius, excluding identified substructure. The sorted eigenvalues of the matrix represent the squares of the principal ellipsoid axes, where a >b >c. **[ASV: Not sure if I should include the equation for the mass distribution tensor.] [ARZ: Yes, put in the equation. Also, I don't think your statement about rockstar excluding substructure is accurate. Is it? Please check on this.][ASV: I am entirely sure that for the shape parameters substructure is excluded**

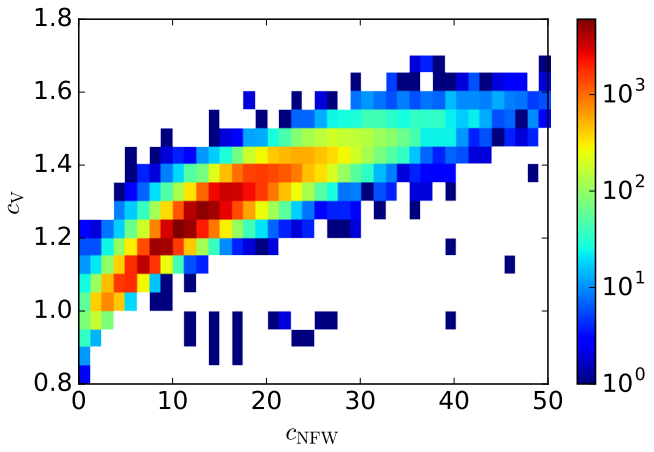

Figure 3. The relationship between the two different measures of concentration, using halos in L0250. The color scale, shown at the right, encodes the number of halos within a single two-dimensional bin in the $c_{\rm NFW}$-$c_{\rm V}$ space. The red (blue) regions on the plot show where the most (fewest) halos exist with those values of the two concentration parameters. The white regions indicate where no halos hold these values. The scatter on this relationship ranges from 5% for intermediate concentration values, to a high of 13% at high masses.

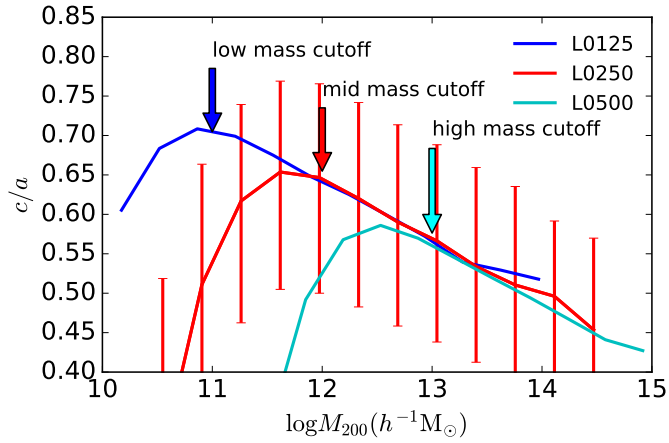

Figure 4. The relationship between the halo shape and halo mass for each of our simulations with $\Delta = 200$. In order of increasing simulation volume, the blue line corresponds to the shape-mass relation from simulation L0125, the red line corresponds to L0250, and the cyan line corresponds to L0500. The red error bars show the 68% spread in parameter values within that mass bin for L0250. These errors are comparable to those of the other simulations within the region of interest. Each simulation is subject to resolution limitations at different halo masses. We show with arrows the minimum M_{200} mass thresholds that we adopt in our analyses using the same color code as the shape-mass relations, going from L0125 to L0500 from left to right. The mass cutoffs chosen for this mark are at higher masses in order to account for the additional number of particles needed to properly measure the halo shape. Note the deviation from a monotonic trend as a result of resolution effects.

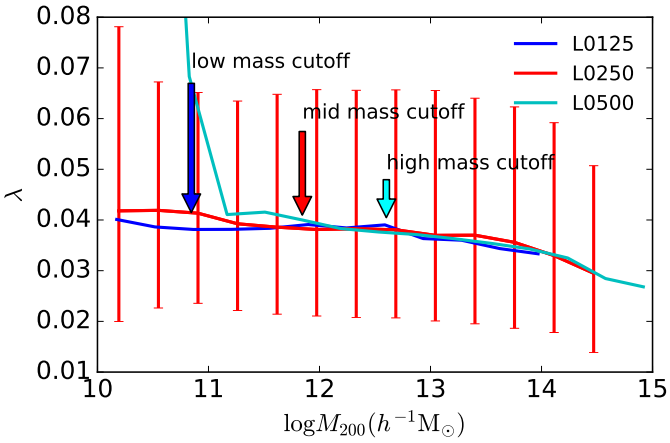

Figure 5. The relationship between the halo spin and halo mass for each of our simulations with $\Delta = 200$. In order of increasing simulation volume, the blue line corresponds to the spin-mass relation from simulation L0125, the red line corresponds to L0250, and the cyan line corresponds to L0500. The red error bars show the 68% spread in parameter values within that mass bin for L0250. These errors are comparable to those of the other simulations within the region of interest. Each simulation is subject to resolution limitations at different halo masses. We show with arrows the minimum M_{200} mass thresholds that we adopt in our analyses using the same color code as the spin-mass relations, going from L0125 to L0500 from left to right. Note the deviations from the near linear trend at low mass due to resolution effects.

by ROCKSTAR.] The mean relations for halo shapes as a function of halo mass for $\Delta = 200$ are shown in Figure 4 along with the mass thresholds used to ensure that our results are not compromised by resolution.

3.3 Halo Spin

We study halo clustering as a function of halo angular momentum quantified by the spin parameter, λ, as introduced by (Peebles 1969),

$$\lambda = \frac{J\sqrt{|E|}}{GM_{\Delta}^{2.5}} \tag{7}$$

where J is the halo angular momentum, E is the total energy of the halo, and M_{Δ} is the mass at the halo radius, r_{Δ}. We measure this quantity using ROCKSTAR which calculates the angular momentum, total energy, and total mass within Δ using bound particles out to the corresponding halo radius. The mean relations for halo spin as a function of halo mass for $\Delta = 200$ are shown in Figure 5 along with the mass thresholds enforced to ensure that our results are not compromised by resolution. These thresholds are summarized in Table 1, where we also show the threshold masses at various values of the overdensity parameter, Δ.

3.4 Halo Samples

In practice, the mean relations between the various halo properties and the mass thresholds for our analyses must be determined separately for each combination of simulation, halo property (e.g., $c_{\rm NFW}$ or s), and halo definition (i.e., value of Δ in the case of the present study). For each analysis, we set mass thresholds in order to avoid the regime in which halo parameters are not well measured due to resolution limits of the simulations; we draw attention to the downturn in Figure 1 as an example of this, as the deviation from the underlying monotonic trend shifts with the change in simulation from lower to higher resolution, suggesting that this is the result of resolution alone.

For ease of comparison between halo definitions, we choose to use a single mass threshold for each simulation and value of Δ whenever possible, rather than on a parameter-by-parameter basis. The one exception to this method is the mass thresholds chosen for the halo shape parameter. This parameter requires a larger number of particles to be well measured; we direct attention to the downturn in Figure 4, which occurs at a significantly higher mass than demonstrated with other halo properties (see Figure 1 for comparison). We analyze the shape parameter with separate, larger minimum mass thresholds to account for the requirement for a larger number of particles. This allows us to have better signal-to-noise in the remaining parameters, while avoiding drawing potentially erroneous conclusions when analyzing the halo shape parameter. We summarize the mass thresholds we have used for a subset of Δ values in Table 1. At most values of Δ, the minimum mass thresholds are driven by the requirement that the halo properties do not suffer sig-

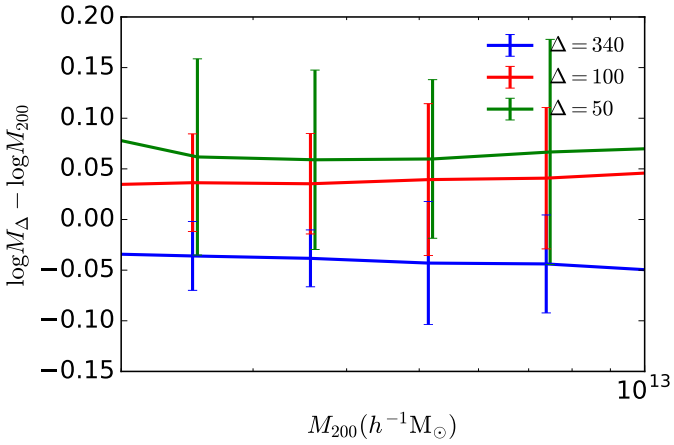

Figure 6. The logarithmic difference between host halo mass for a given definition of Δ and the equivalent halo for a definition of $\Delta = 200$ in logarithmic space. The blue (red, green) lines look at the ratio with respect to the values of $\Delta = 340$ $(100, 50)$. Error bars show one standard deviation of the distribution in that mass bin. Note that while the expectation is that the halo mass will be larger for lower values of Δ, there are some differences due to differences in halo identification. **[ARZ: Several comments. First, plot $\log(M_\Delta/M_{200})$ because M_{200} is the quantity people will be familiar with. Second, you should compute these ratios from the "matched" catalogs! That way there is no issue of having the ratio affected by including or excluding certain halos. Third, you have to specify what the lines and errorbars are? Are they mean and scatter? Lastly, I think it is best if the x-axis is logarithmic. Most of your data is piled up against the y-axis here because that is where most of yourh halos are! A logarithmic x-axis running from $\sim 10^{11}$ to $\sim 10^{14}$ seems most sensible to me.]**

nificantly from finite resolution effects. We alert the reader to the fact that the mass of an individual halo will vary as Δ varies. This effect can be seen in Figure 6, which demonstrates that while a decreased value of Δ leads to larger masses on average, there is a scatter due to changes in halo identification. Roughly speaking, the threshold masses in Table 1 vary in such a way that the same physical objects are selected at each halo definition.

4 HALO CLUSTERING AS A FUNCTION OF AUXILIARY HALO PROPERTIES

4.1 Auxiliary Halo Properties and Their Mass Dependence

We are interested in studying the clustering behavior of halos as a function of properties other than mass. As mass is the dominant halo property determining halo clustering strength and environment, we refer to the other properties that we study as "auxiliary halo properties" (those properties other than mass, such as concentration $c_{\rm NFW}$ or shape s). As has been demonstrated extensively in the literature, the auxiliary properties that we consider are themselves a function of mass (Bullock et al. 2002; Allgood et al. 2006; Duffy et al. 2008; Despali et al. 2016). This mass dependence, if not accounted for, induces clustering that depends upon these auxiliary properties in the absence of assembly bias. Most contemporary cosmological N-body simulations, and specifically the suite of simulations that we study in this work, do not have a sufficiently large number of halos to make isolating halos of fixed mass, and then further splitting these halos by an auxiliary property, a statistically powerful method with which to study the dependence of clustering on auxiliary properties. Therefore, it is necessary to remove and/or mitigate the mass dependence of the auxiliary properties that we study.

We mitigate the mass dependence of the auxiliary properties as follows. First, we take all host halos more massive than our minimum mass thresholds and sort them by their halo masses, M_Δ. We place these halos into twenty logarithmically-spaced bins of halo mass, ensuring that no bin has fewer than 10 halos, with the exception of the most massive bin. The objects in this final bin are rare and exceptional enough that they have little statistical value and do not influence our results considerably. We then calculate the rank of each auxiliary property within the bin of halo mass, from 1 to N, where N is the number of halos assigned to a given bin. If multiple halos share auxiliary property values (e.g. rank 2 and 3 have the same halo shape), then the average value of the rank is assigned to each halo (e.g. 2.5 to each). We normalize the rank distribution to be between 0 and 1 by dividing out the number of halos in the bin. This removes the strong mass trend in each of these properties. We use these normalized ranks of halo auxiliary properties to study halo clustering strength in the remainder of this work. We have experimented with different bin sizes. We find that our qualitative results are not sensitive to the number of bins we use. Furthermore, the choice of equally populated bins versus evenly spaced bins makes no significant difference to our results.

In addition to the properties of the host halos described in the previous section, we also study the strength of halo clustering as a function of subhalo number. Host halo size and the number of satellite halos (above some threshold in a proxy of satellite halo size) are also strongly correlated. Roughly speaking, the number of satellite halos above a fixed size threshold grows in approximate proportion to host halo mass Zentner et al. (2005). **[ARZ: Cite Kravtsov et al. 2003 here.]**

To account for the correlation between halo mass and abundance of subhalos, we follow the prescription of Wechsler et al. (2006). We first select all subhalos from the sample that meet the criterion that the ratio $V_{\rm max,sub}/V_{\rm max,host} \geq 0.3$, where $V_{\rm max,sub}$ and $V_{\rm max,host}$ are the maximum circular velocities of the subhalos and host halos respectively. This choice of scaling exploits the fact that the subhalo velocity function is a very nearly self-similar function (Zentner et al. 2005) so that the scaling eliminates the gross mass dependence of satellite number. **[ASV: need to add in additional citations here.]** In addition, this choice of threshold will mean that for subhalos above the resolution threshold of the simulation, there shall be of order a few satellite halos per host on average. We then choose a threshold for the host maximum circular velocity such that all subhalos are well-resolved in the simulation volumes: 135, 235, and 400km s^{-1} for L0125, L0250, and L0500 respectively. Subhalo maximum circular velocities were used as a proxy for subhalo size rather than subhalo masses because subhalo maximum

Table 1. Minimum mass thresholds for each of our analyses. In the columns below each value of Δ, we show the minimum host halo masses considered in units of $h^{-1}\mathrm{M}_{\odot}$. Those rows without a label of "-shape" refer to the mass cut chosen for all analyses other than halo shape. Those rows with a label of "-shape" refer to the mass cut chosen for the shape parameter analyses. The latter require higher mass thresholds.

Cutoff Name	$\Delta = 340$	$\Delta = 200$	$\Delta = 100$	$\Delta = 75$	$\Delta = 50$	$\Delta = 10$
low mass	6×10^{10}	7×10^{10}	8×10^{10}	9×10^{10}	1×10^{11}	2×10^{11}
low mass-shape	2×10^{11}	2×10^{11}	2×10^{11}	2×10^{11}	2×10^{11}	2×10^{11}
mid mass	6×10^{11}	7×10^{11}	8×10^{11}	9×10^{11}	2×10^{12}	N/A
mid mass-shape	2×10^{12}	2×10^{12}	2×10^{12}	2×10^{12}	2×10^{12}	N/A
high mass	3×10^{12}	4×10^{12}	5×10^{12}	6×10^{12}	7×10^{12}	N/A
high mass-shape	1×10^{13}	1×10^{13}	1×10^{13}	1×10^{13}	1×10^{13}	N/A

circular velocities can be more robustly measured from simulation data, making comparison to other work easier. Once these cuts have been applied, we again divide the halos that meet these cutoffs into bins in logarithmic halo mass and follow the same procedure as with the other auxiliary halo properties. **[ARZ: Now that you use ranks, this means you are "doubly" removing the mass dependence. This is OK. It just may not be necessary now that you have moved to using ranks.][ASV: Probably not necessary, though it does serve as an informed cut on minimum subhalo mass, so I will leave it in.]**

4.2 Clustering Statistics

We assess the influence of assembly bias specifically on two-point statistics of host halos. In order to do so, we study both the standard two-point correlation functions of halos selected by properties other than mass (e.g., the auxiliary properties concentration, shape, and spin) as well as halo mark correlation functions (MCFs). MCFs quantify the manner in which a halo property (the "mark") correlates among halo pairs as a function of the distance between the pairs. MCFs have the advantage that they effectively stack signal from all values of the halo auxiliary property, or mark, in contrast to selecting subsets of halos based on the auxiliary property. MCFs also stack signal from all environments and do not require any specific definition of halo environment in order to detect "environmental" trends that are usually referred to as assembly bias in the literature. Absent halo assembly bias, the halo marks are uncorrelated among pairs. MCFs have been used in many previous papers to quantify environmental dependence of halo properties other than mass (Sheth & Tormen 2004; Sheth 2005; Harker et al. 2006; Wechsler et al. 2006; Mao et al. 2015). Although it does not necessarily have to be the case, we find that using correlation functions of halo sub-samples and using MCFs lead to the same broad conclusions.

For a specific halo property, or mark m, we use the MCF normalization of Wechsler et al. (2006), namely

$$\mathcal{M}_m(r) \equiv \frac{\langle m_1 m_2 \rangle_p(r) - \langle m \rangle^2}{\mathcal{V}(m)}, \qquad (8)$$

where m_i is the value of the mark for halo i, $\langle m \rangle$ is the mean of the mark, and $\mathcal{V}(m)$ the variance of the mark. The notation is intended to indicate that the average is taken over all pairs of halos separated by a distance r. In the absence of any correlation between a halo property among neighbors a separation r away, $\mathcal{M}_m(r) = 0$. Deviations of the MCF from zero indicate such correlations exist and the magnitude of $\mathcal{M}_m(r)$ gives the excess of the mark among pairs compared to the one-point mean of the mark $\langle m \rangle$ in units of the one-point variance. The marks that we use are the normalized ranks of halo auxiliary properties described in Section 4.1. Therefore, these marks are distributed according to a uniform distribution from 0 to 1, so that $\langle m \rangle^2 = 0.25$ and that $\mathcal{V}(m) = 1/12$.

In each case, it is necessary to assess statistical fluctuations in the statistics that we measure in these simulations in order to determine the significance of the signals. For two-point correlation functions, we determine the covariance of the measurement through jackknife resampling of the eight octants of the simulation cube.

[ARZ: After the discussions that we had, is this still what you are doing?][ASV: No it is not! I missed changing it!] We assess the significance of the MCFs by taking advantage of the inherent uniform distribution. For each halo we assign a random mark drawn from a uniform distribution. We repeat this process 200 separate times and calculate the MCF for each set of random marks. From this distribution of MCF values, we take the 2% and 98% percentile values in order to create a range which should correspond well with a 2 σ interval; we propose that a signal within this range could not be positively identified as assembly bias. We note that since we investigate the product of two uniformly distributed variables, a negative value of the MCF has two different interpretations. One interpretation is that halos with high (low) values of the mark experience enhanced (diminished) clustering. The other possible interpretation is an enhanced clustering of high value marks with low value marks. While we cannot distinguish between these two possibilities, it does not impact our ability to make statements about a potential non-detection of assembly bias, as our randomization implicitly accounts for the impact of a uniform product distribution.

5 RESULTS

5.1 Correlation Functions

We begin by studying the correlation functions of halos in our mass threshold samples, sub-selected by auxiliary properties. Figure 7 exhibits the difference between the clustering strength of halos in the $20^{\rm th}$ percentile highest NFW concentrations and the halos with the halos that have the $20^{\rm th}$ percentile lowest NFW concentrations as a function of the overdensity parameter, Δ, used to define the halos. In order to make the differences more apparent, the two-point functions in Fig. 7 have been normalized by the clustering strength of the entire halo sample.

If the clustering strength of halos were independent of halo concentration, we would expect the lines in Fig. 7 to cluster around zero (scattered about zero by finite sample size). The evident deviations demonstrate that halos of different NFW concentrations exhibit appreciably different clustering, a fact that is already well known and has been studied by a number of authors. Furthermore, it is clear that the strength and sign of assembly bias due to NFW concentration is strongly mass dependent for any fixed halo definition, a result that also agrees with the significant previous literature on halo assembly bias using conventional halo definitions (Wechsler et al. 2002; Gao et al. 2005; Zentner 2007; Wechsler et al. 2006; Harker et al. 2006; Croton et al. 2007; Dalal et al. 2008; Mao et al. 2015; Sunayama et al. 2016). At relatively low mass (the low-mass panel, $M_{200} > 7 \times 10^{10}\ h^{-1}{\rm M}_{\odot}$), high-concentration halos are considerably more strongly clustered than low-concentration halos using the more conventional $\Delta = 200$ definition for halos. At somewhat higher halo masses (e.g., the mid-mass panel, $M_{200} > 7 \times 10^{11}\ h^{-1}{\rm M}_{\odot}$), this difference is markedly reduced. Finally, for the highest-mass halos that we have the capability of studying (the high-mass panel, $M_{200} > 4{\times}10^{12}\ h^{-1}{\rm M}_{\odot}$), the effect is weaker and also of opposite sign; low-concentration halos are more strongly clustered than high-concentration halos.

Focus, for example, on the middle panel of Fig. 7. In this panel, corresponding to the mid-mass threshold, the difference in large-scale clustering between high- and low-concentration halos is dramatically reduced for a halo definition with $\Delta \approx 60$ as compared to a more traditional halo definition, such as $\Delta = 200$. However, further decreasing Δ leads to concentration-dependent clustering of opposite sign. Both the strength and the sense of halo assembly bias depend upon halo definition! This is a point that may seem somewhat obvious in retrospect, but does not seem to be addressed explicitly anywhere in the literature despite its importance.

Comparing the differing clustering strengths across the three panels of Fig. 7, it is clear that any specific conclusions about concentration-dependent halo clustering vary with halo mass. For low-mass halos (the top panel), very low values of Δ (and correspondingly large definitions of halo radii, as R_{Δ} very roughly in proportion to $\Delta^{-1/3}$) are necessary in order to mitigate the concentration dependence of halo clustering. Conversely, for higher-mass halos (the bottom panel), conventional values of $\Delta \sim 200 - 340$ yield little concentration-dependent clustering. In this case, decreasing Δ (increasing R_{Δ}) results in significantly *increased* concentration dependent halo clustering. The reasons for these changes are of interest and we return to the interpretation of these results below.

Notice that in all panels of Fig. 7, the effect of concentration-dependent clustering is mildly scale-dependent. Moreover, this scale dependence is evident for all values of Δ. Simply defining halos with a different value of Δ does not suffice to eliminate concentration-dependent clustering on all scales. In this discussion and throughout, we focus primarily on the large scale clustering, which we take to mean clustering on scales significantly larger than the radii, R_{Δ} of the halos in our samples.

It should be noted that this method is robust to the choice of samples. For instance, changing from examining the $20^{\rm th}$ percentile of concentrations to another value (e.g., $10^{\rm th}$ or $50^{\rm th}$ percentile) does not change the conclusions drawn from Fig. 7 significantly. In the case of halo concentration, adopting $c_{\rm V}$ rather than $c_{\rm NFW}$ also does not alter our conclusions. Therefore, we do not show these additional results in the interest of brevity.

Furthermore, we note that quite generally, for each of the halo properties we have studied, the conclusions drawn from examining correlation functions are the same as those drawn from studying MCFs. Consequently, we now move on to a more comprehensive discussion of the strength of auxiliary property-dependent halo clustering using MCFs.

5.2 Mark Correlation Functions

5.2.1 Halo Concentration

The NFW concentration, $c_{\rm NFW}$, MCF is shown in Figure 8. The shaded bands in the figure delineate the statistical fluctuations in MCFs induced by finite sampling as discussed in Section 4.2. Qualitatively, Fig. 8 exhibits the same features that are evident in Fig. 7: more concentrated halos are significantly more clustered in the low-mass cut L0125 halo sample; concentration-dependent halo clustering weakens and reverses sense as halo mass increases (at fixed Δ), consistent with work on assembly bias (Wechsler et al. 2006; Sunayama et al. 2016); for the mid-mass cut L0250 sample with $\Delta = 60$, the large-scale concentration dependence of halo clustering has been reduced so as to be consistent with zero within the statistical limitations of the simulation.

Figure 9 is a similar plot for the MCF of the velocity-ratio concentration, $c_{\rm V}$. This figure exhibits qualitatively very similar features to Fig. 8, a fact that is not surprising given that we already know that $c_{\rm NFW}$ and $c_{\rm V}$ quantify largely redundant information about their halos.

5.2.2 Halo Shape

[ARZ: A few comments here on the shape disussion and on Figure 10. First, does your discussion really go with what is shown in the plot? I see that going down to $\Delta = 20$ helps A LOT. Related to this, the red dashed lines in the middle and bottom panels don't make sense? They are clearly not the best case scenarios. In fact, it looks to me like the best case should be $\Delta = 20$ in ALL PANELS! Am I missing something? Finally, you don't discuss Figure 11 AT ALL in the paper? Is it necesssary? I think probably not?] [ASV: Added in lines about

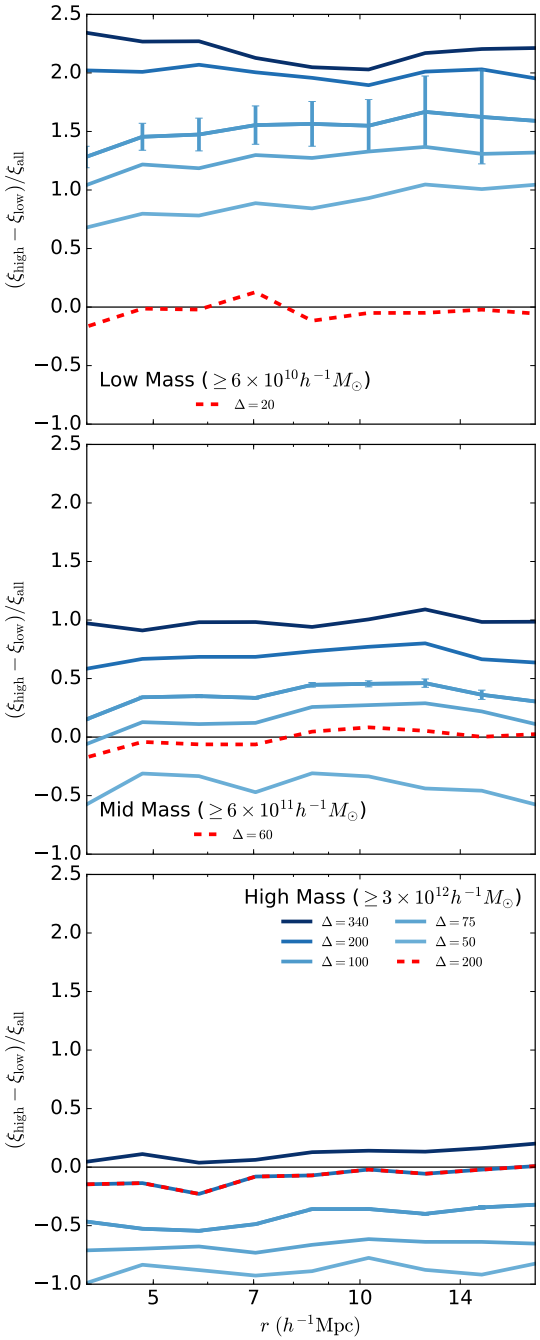

Figure 7. In each panel, the solid lines plot the difference between the correlation function for the top 20% and the bottom 20% of halos by NFW concentration, normalized by the correlation function of the entire sample. In each plot the lines correspond to different values of Δ, with dark blue (light blue) corresponding to $\Delta = 340$ ($\Delta = 50$). The line corresponds to the overdensity chosen for matching as possibly removing assembly bias on most scales in the case of halo concentration. The top (middle/bottom) panel shows the results for the L0125 (L0250/L0500) data set utilizing the low mass (mid mass/high mass) cutoffs. Error bars correspond to the two σ error on the measurement.

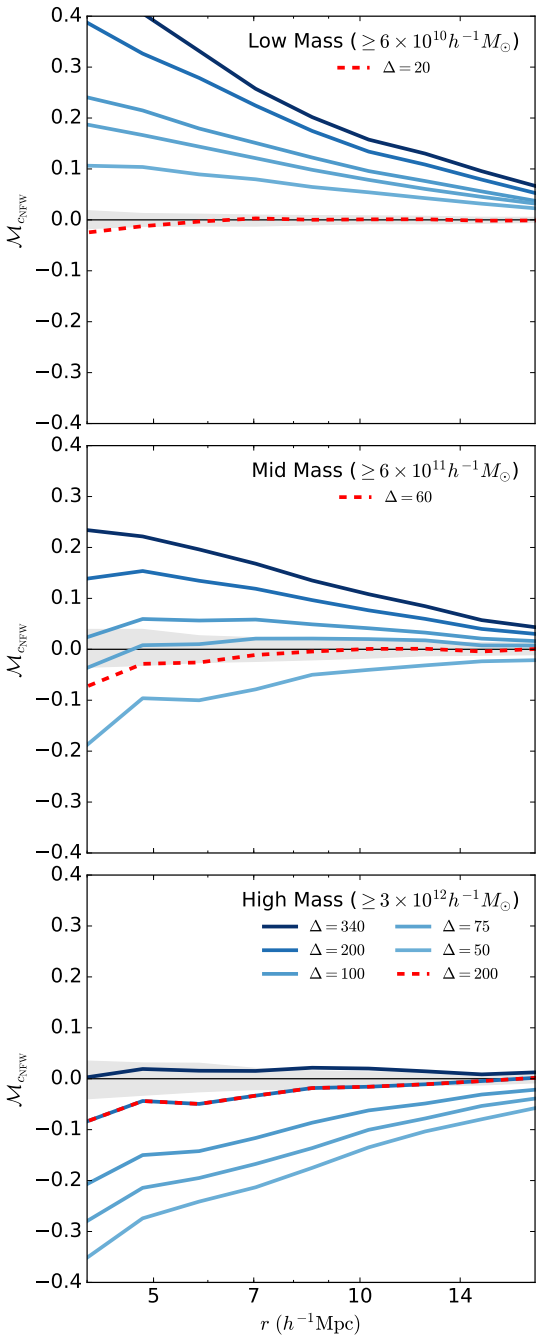

Figure 8. The marked correlation function for the concentration defined according to the NFW profile. The solid lines plot the marked correlation function using normalized ranks of NFW concentration as the mark. In each plot the lines correspond to different values of Δ, with dark blue (light blue) corresponding to $\Delta = 340$ ($\Delta = 50$). The red dashed line corresponds to the overdensity chosen for matching as possibly removing assembly bias on most scales in the case of halo concentration. The top (middle/bottom) panel shows the results for theL0125 (L0250/L0500) data set utilizing the low mass (mid mass/high mass) cutoffs. The shaded bands represent 2-sigma confidence regions generated by randomization of the marks.

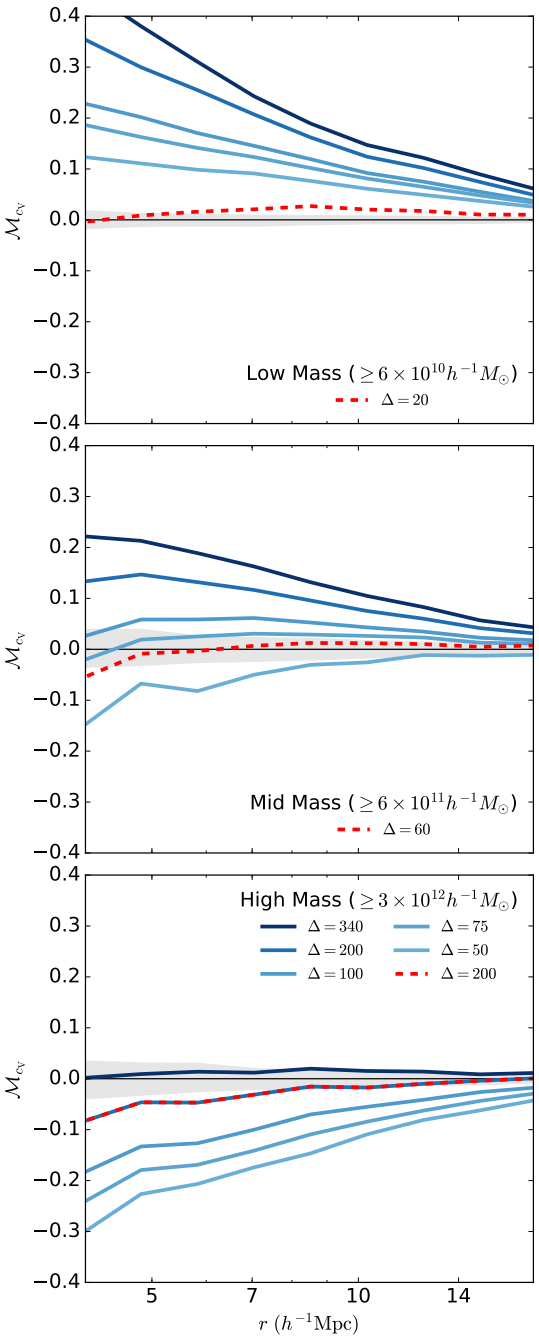

Figure 9. The marked correlation function for the concentration defined according to the ratio of maximum circular velocities. The solid lines plot the marked correlation function using velocity ratio concentration as the mark. In each plot the lines correspond to different values of Δ, with dark blue (light blue) corresponding to $\Delta = 340$ ($\Delta = 50$). The red dashed line corresponds to the overdensity chosen for matching as possibly removing assembly bias on most scales in the case of halo concentration. The top (middle/bottom) panel shows the results for the L0125 (L0250/L0500) data set utilizing the low mass (mid mass/high mass) cutoffs. The shaded bands represent 2-sigma confidence regions generated by randomization of the marks. **[ARZ: Still have to play with the cosmetics of this plot a little. Too much data is cut our of the top panel. Maybe extend the vertical axis to about 0.4 or so? Then it would have the same dynamic range as the NFW concentration plot, which would be nice!][ASV: Changes made!]**

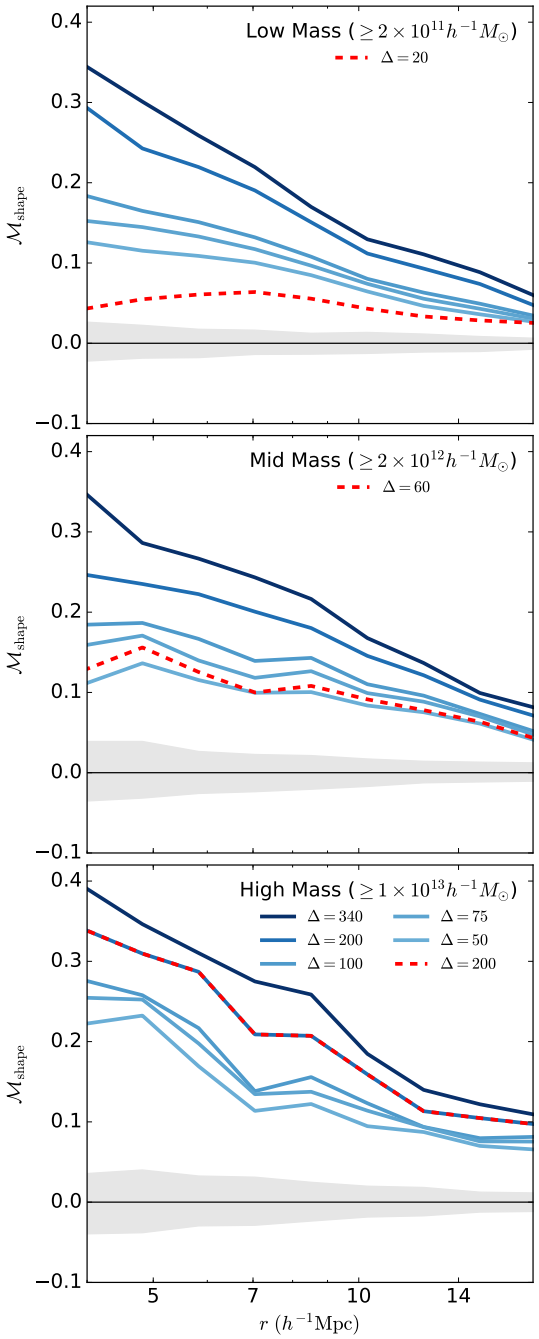

Figure 10. The marked correlation function for the halo shape parameter. In each plot the lines correspond to different values of Δ, with dark blue (light blue) corresponding to $\Delta = 340$ ($\Delta = 50$). The red dashed line corresponds to the overdensity chosen for matching as possibly removing assembly bias on most scales in the case of halo concentration. The top (middle/bottom) panel shows the results for the L0125 (L0250/L0500) data set utilizing the low mass-shape (mid mass-shape/high mass-shape) cutoffs. The shaded bands represent 2-sigma confidence regions generated by randomization of the marks.

how our red dashed lines are best case with regards to halo concentration. I also will remove the figure on how shape evolves with Δ - that was more relevant when we were getting shape measurements that were anomalous with previous paper results.] Moving on from concentrations, Figure 10 illustrates MCFs in which the mark is the normalized rank of the shape parameter, s, of the halo. Similar trends as the previous cases repeat themselves in the case where shape is used at the trace mark. For the entire range of halo masses studied, the fiducial halo definition shows that more clustered halos have more spherical halos (e.g. halos with larger s values). Furthermore, our change in halo definition shows that increasing the size of halos (and decreasing Δ) leads to the most clustered halos having less spherical halos.

Where the environmental dependence associated with the shape parameter distinguishes itself is in finding the best fit value of Δ for removing the halo assembly bias. No reasonable value of Δ seems to be capable of removing the enhanced clustering at the scales that we study, though the impact is reduced. We note that the best fit matches for concentration, the red-dashed lines in Figure 10, do not correspond with removing assembly bias from shape. This failure may be driven by the filamentary nature of large-scale structure. Halos in overdense regions will gain mass as their halo radius expands that is not associated as substructure. If this additional mass accumulates with a preferred direction, as may be expected along a filament, this could induce a more elliptical halo shape. A detailed test of this hypothesis is beyond the scope of this paper, but may well be testable through association of halos with large-scale structure.

It should be noted that the process by which ROCKSTAR calculates shape does inherently exclude substructure. Since subsumed host halos are identified as substructure in catalogs with lower values of Δ, their mass is not included in the calculation of halo shapes. While beyond the scope of this work, it is possible that inclusion of substructure into our halo shape calculations could result in an improved reduction of assembly bias. This may merit future investigation.**[ASV: Or so I propose. I figure that this requires full particle data or a modification to ROCKSTAR. It would be valuable to do, but would delay the paper more than I care to sort out in the meantime. That being said, if it does work for spin, it would be important to know about.]**

5.2.3 Halo Spin

[ARZ: Spin-dependent clustering does NOT give qualitatively the same results as shape-dependent clustering. This paragraph needs to be re-written. And again, in Fig. 11, the red dashed lines do not make sense to me. They are clearly NOT the best choices for the case of spin.][ASV: Some incorrect holdovers here. Fixing now.] The spin MCFs are shown in Figure 11. Halos that are more clustered show higher values of the spin mark than would be expected from a uniform distribution of ranks. As with halo shape, it can be seen that the best match for halo concentration (the red-dashed lines in Figure 11) are poor fits for removing assembly bias from halo spin.**[ARZ: Search the literature, particularly Brandon Allgood's papers and Andreas Faltenbacher whose names come to mind, for spin-dependent assembly bias. I'm trying to figure out if yours is the first paper to point this out.][ASV: Need to track down all the specific citations, but after changing our normalization method, it seems to match up better with existing texts.] [ARZ: Citations here still need to be done.]** However, halo spin shows a qualitative response to our methodology which is opposite from previous results. Increasing halo radii by decreasing Δ only serves to increase the impact of assembly bias in this case; effectively our newly defined halos have higher spins than average in this case. As with halo shape, one can invoke a model relating back to filamentary structure. If new material is accumulated along some preferred direction, it is not unreasonable to conclude an increased value of spin. This might enhance the impact of assembly bias as a result of our method.

5.2.4 Subhalo Abundance

The clustering of halos as a function of the number of satellite galaxies at fixed mass is of particular practical interest. Efforts to model survey data on the large-scale galaxy distribution, such as the halo occupation distribution (HOD) or conditional luminosity function (CLF) formalisms typically make the assumption that the multiplicity of satellite galaxies within a host dark matter halo depends solely upon halo mass. If this assumption is violated, then the phenomenological modeling of galaxy clustering can be more complicated than in these simplest scenarios.

[ARZ: Same comments here as with spin and shape. Red dashed lines are clearly not the best choices. I don't know what you are trying to illustrate with them?][ASV: Changes made to the caption and mention in the text.] Figure 12 shows clustering marked by satellite number as described in § 4. For all values of Δ, halo clustering is strongly dependent upon satellite occupation at all masses. We note that as we move to higher masses, the most clustered halos have higher satellite occupations. Once again we note that the halo definition that removes assembly bias from halo concentration does not serve as a good definition for satellite occupation. As with halo spin, defining halos to have larger radii (smaller Δ) generally makes the environmental dependence of halo clustering more significant. Of course, our results pertain to satellite halos, or subhalos, rather than satellite galaxies, so the connection to observations and how one might model observed galaxy clustering is indirect, yet suggestive. We also note that the fact that the clustering appears reduced at lower masses is qualitatively in agreement with the predictions from Wechsler et al. (2006).

6 DISCUSSION

6.1 General

We have studied the clustering of dark matter halos as a function of halo properties other than mass. We have confirmed that for conventional halo definitions halo clustering strength is a strong function of the "auxiliary properties"

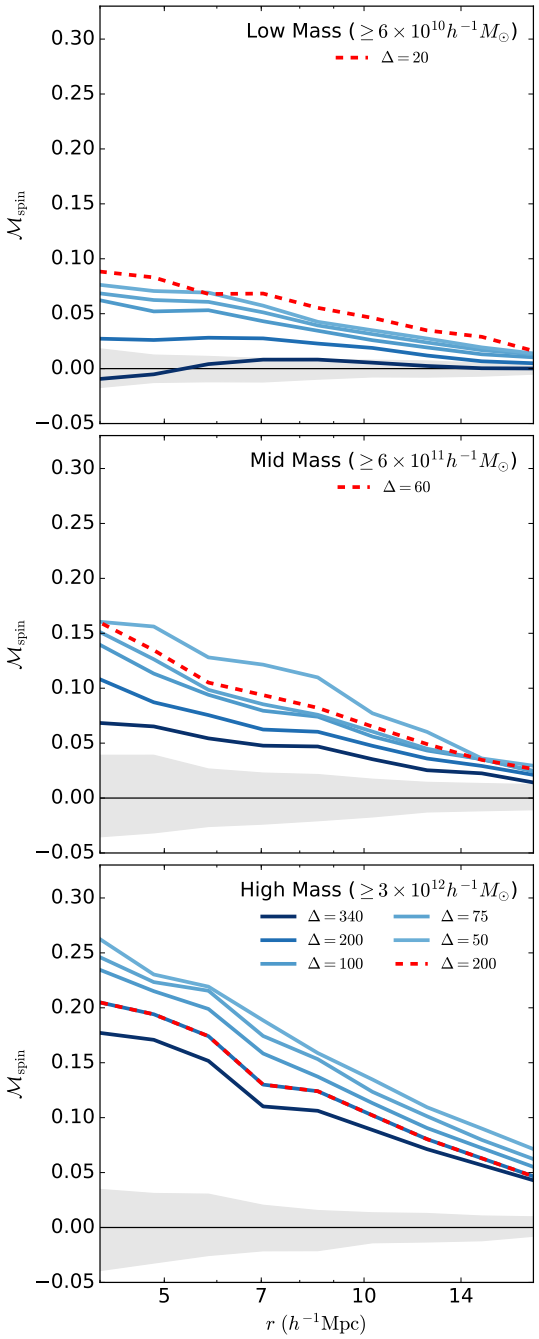

Figure 11. The marked correlation function for the halo spin parameter. The solid lines plot the marked correlation function using halo spin as the mark. In each plot the lines correspond to different values of Δ, with dark blue (light blue) corresponding to $\Delta = 340$ ($\Delta = 50$). The red dashed line corresponds to the overdensity chosen for matching as possibly removing assembly bias on most scales for halo concentration. The top (middle/bottom) panel shows the results for the L0125 (L0250/L0500) data set utilizing the low mass (mid mass/high mass) cutoffs. The shaded bands represent 2-sigma confidence regions generated by randomization of the marks.

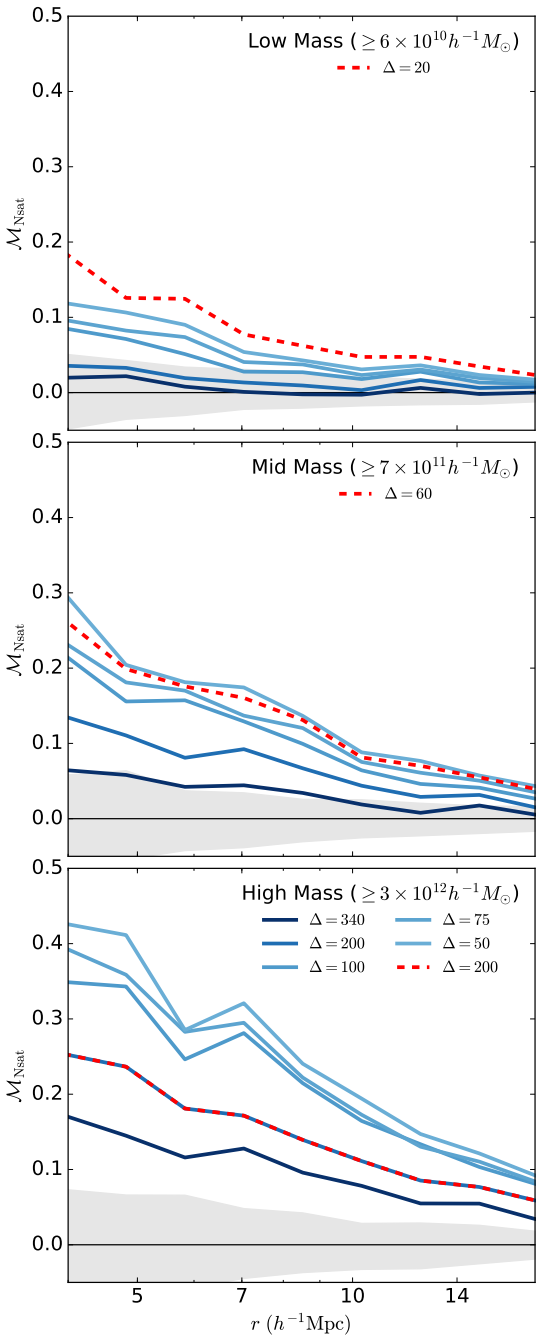

Figure 12. The marked correlation function for the satellite number parameter. The solid lines plot the marked correlation function using halo satellite number as the mark. In each plot the lines correspond to different values of Δ, with dark blue (light blue) corresponding to $\Delta = 340$ ($\Delta = 50$). The red dashed line corresponds to the overdensity chosen for matching as possibly removing assembly bias on most scales for halo concentration. The top (middle/bottom) panel shows the results for the L0125 (L0250/L0500) data set utilizing the low mass (mid mass/high mass) cutoffs. The shaded bands represent 2-sigma confidence regions generated by randomization of the marks.

that we studied, namely halo concentration (either measured through a fit to the NFW profile or assigned nonparametrically as the ratio of the maximum circular velocity to the virial velocity), halo shape, halo spin, and substructure content. These findings are consistent with the now significant literature on the subject subject of halo assembly bias. (Peacock & Smith 2000; Wechsler et al. 2002; Sheth & Tormen 2004; Gao et al. 2005; Zentner et al. 2005; Allgood et al. 2006; Harker et al. 2006; Wechsler et al. 2006; Croton et al. 2007; Zentner 2007; Dalal et al. 2008; Zentner et al. 2014; Mao et al. 2015; Sunayama et al. 2016)

We have explored auxiliary property dependent halo clustering as a function of halo definition, parameterized by overdensity parameter Δ. This exploration was motivated, in part, to determine whether alternative halo definitions can mitigate the dependence of halo clustering on these "auxiliary properties." In general, we find that these alternative definitions do *not* significantly mitigate the effects of assembly bias. Moreover, these modified halo definitions, with low values of Δ, often lead to stronger assembly bias, rather than weaker assembly bias. Concentration-dependent clustering is an exception to this conclusion that we will discuss further below.

An interesting and general conclustion that follow from our work is that auxiliary property dependent halo clustering, or assembly bias, depends greatly on halo definition. In each of Figures 8 through 12, the strength of assembly bias is a strong function of halo definition. This definition dependence is not restricted to extreme choices of the overdensity parameter Δ. The difference in the strength of assembly bias between a "virial" halo definition, with $\Delta = 340$, and a definition with $\Delta = 200$ is considerable. Indeed, the difference can even lead to a difference in the *sense* of the assembly bias; higher concentration halos may be more strongly clustered by one halo definition and more weakly clustered by another. It is interesting to consider that differences on the strength of assembly bias in the literature may be partly induced by the different halo definitions used by different authors.

6.2 Mitigating Concentration-Dependent Clustering with Halo Definition

Our results suggest that halo redefinition may be able to mitigate concentration dependent halo clustering. This is evident in Fig. 8 and Fig. 9. Halo concentration is strongly correlated with halo formation time, so this suggests that such a redefinition *may* aid in reducing assembly bias associated with halo formation time; however, this is a non-trivial extrapolation of our results and a follow-up study to assess halo formation times in alternative halo definitions is both interesting and warranted.

Clearly, the halo definition that best mitigates concentration-dependent assembly bias must be mass dependent. Low values of Δ ($\Delta \sim 25$ with $R_{25} \sim 2R_{200}$) seem appropriate near for our lowest mass-threshold sample (with $M_{200} \geq 7 \times 10^{10}\ h^{-1}\mathrm{M}_{\odot}$) whereas $\Delta \sim 200$ or slightly higher is adequate for our highest mass threshold sample (with $M_{200} \geq 4 \times 10^{12}\ h^{-1}\mathrm{M}_{\odot}$).

This result is reminiscent of much recent work on the so-called halo "splashback radius" (More et al. 2015) and, indeed, our efforts were partly motivated by this work. We note that while the splashback radius methodology does seem similar in concept to our methodology, Fig. 13 demonstrates that a one-to-one comparison between the two methods is difficult at best. While both our method of halo redefinition and their determination of splashback radius seem to show a monotonic trend in mass, we note that our work with the lowest mass halos requires a definition of halo radius that substantially larger than the splashback radius method alone might suggest.

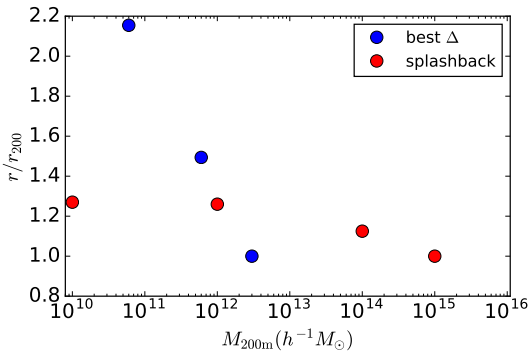

Figure 13. A comparison of the average ratio between r_{200} and the splashback radius as determined by More et al. (2015) (red circles) to the average ratio between r_{200} and the halo radius determined as our best fit for removal of assembly bias as discussed above (blue circles). Note that the halo mass chosen for the blue points is determined by the mass cutoff in the simulation analysis, as the smallest (and most numerous) halos dominate the calculation.

It is useful to investigate the reasons why halo redefinitions may be helpful in the case of concentrations. On the positive side, it is possible that these redefinitions do define halos an a more practically useful way, better isolating objects that have been strongly altered by nonlinear evolution from the larger-scale environment. In this case, halo redefinition would be a step forward. However, it is also possible that the details of measuring halo properties using these new halo definitions introduce new sources of noise into the measurements. If this is the case, then the reduction in environmental effects stems from the fact that them measurement of the halo property introduces noise and is *less* informative about the halo itself. For the case of halo concentration, which is the most interesting to follow up, introducing noise can happen in numerous ways. For example, the NFW concentration c_{NFW} is determined by a fit to the NFW profile. Inferred values of c_{NFW} will depend upon the degree to which the density profiles of the halos follow the NFW functional form within some radius R_{Δ} that is different from traditional halo radii, such as $\sim R_{200}$. At large halocentric distances ($r \gtrsim R_{200}$) halo profiles are known to deviate from the NFW form. It is worth noting that the velocity-defined concentration c_{V} is a non-parametric measure of concentration and should be less subject to such effects.

We note that the mean dispersion of halo concentrations for a given mass bin are not significantly changed as we move to our best fit value of overdensity parameter, Δ. This is highly suggestive of the fact that the success of our method is not the result of larger measurement error, but is more fundamental to the nature of relating halo definition to our halo parameters of interest.**[ARZ: Now you men-**

tion the interesting part about the new figure. This should be a discussion of how much larger/smaller the dispersion in concentrations gets for, say $\Delta = 70$ compared to $\Delta = 200$.] [ASV: The dispersion of halo concentrations is not significantly changed - while a little smaller, it is well within the scatter of the dispersion as well.]

We can explore in more detail the degree to which the mitigation of environmental effects by halo redefinition are due to introducing noise that is uncorrelated with environment into the measurement of halo properties when halos are defined in a manner distinct from the more traditional definitions. We proceed as follows. All host halos that are found in the halo catalogs constructed from lower values of Δ (for example, Δ 60 which is an interesting value for exploring concentration in the mid-mass cut of the L0250 simulation) are present as host halos in the halo catalogs constructed with higher values of threshold density (e.g., $\Delta = 200$). We match each halo in the lower threshold (lower Δ) simulation to its corresponding halo in the higher threshold catalog. We then consider the clustering of only those halos that we have matched across catalogs. We refer to these as the "matched" halo samples between two values of threshold overdensity Δ.

[ARZ: Please check to ensure that I know what you mean by your matched samples. Your language was not specific enough for me to be 100% sure. Modify as necessary.] [ASV: Looks absolutely correct to me.] Figure 14 shows the same statistic as Figure 8, except for matched subsamples. The matched subsamples are matched to a catalog generated for the value of Δ most likely to remove assembly bias at large scales for the concentration marks; $\Delta = 20$ for the 'Low Mass' cut, $\Delta = 60$, for the 'Mid Mass' cut, and $\Delta = 200$ for the 'High Mass' cut. These matched halo catalogs only differ from the standard halo samples in that they contain only those host halos common to both the catalog in question and the best fit Δ catalog. One particularly interesting result is noted in the L0250 data. First draw your attention to the difference between the unmatched (dashed lines) and matched (solid lines) catalog results; this change is driven entirely by the exclusion of host halos due to a change in halo definition, as all other properties are consistent between catalogs. This is highly suggestive that most of the assembly bias signal is driven by the interaction of host halos with other nearby halos. The remaining component of the reduction of assembly bias signal is driven by an increase in noise or some more fundamental difference in how the marks are measured or mass is assigned. We look forward to probing the impact of these effects in the future.

From Fig. 14, it is apparent that some degree of assembly bias persists in the matched samples. Yet, what is interesting is that a very significant fraction of the assembly bias effect has been removed compared to the standard $\Delta = 200$ result. The halos in the matched catalogs have the same properties (including $c_{\rm NFW}$) as those in the standard catalogs, so that removal of assembly bias is *not* due to introducing noise or other systematics into the measurement of concentration. That mitigation of assembly bias is due to the halo redefinition and, in particular, subsuming those halos most subject to assembly bias effects as subhalos of the $\Delta = 70$ halos. This is an interesting result suggesting that seeking optimal halo definitions may be one avenue to

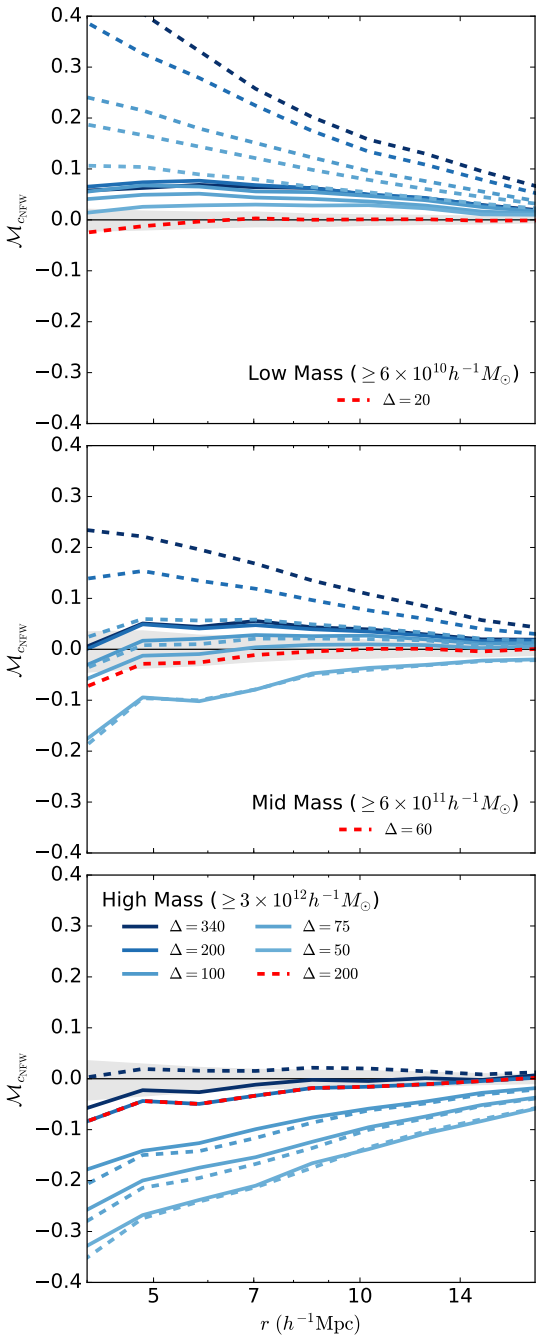

Figure 14. The marked correlation function for the NFW-defined halo concentration parameter. The solid lines plot the marked correlation function using NFW-defined halo concentration as the mark, for a catalog matched against the best fit Δ shown in red. The dashed lines plot the original marked correlation function results. In each plot the lines correspond to different values of Δ, with dark blue (light blue) corresponding to $\Delta = 340$ ($\Delta = 50$). The red dashed line corresponds to the overdensity chosen for matching as possibly removing assembly bias on most scales for halo concentration. The top (middle/bottom) panel shows the results for the L0125 (L0250/L0500) data set utilizing the low mass (mid mass/high mass) cutoffs. The shaded bands represent 2-sigma confidence regions generated by randomization of the marks. Only host halos consistent with the best-fit catalog from above are included in the analysis.

more completely separating the strongly nonlinear evolution occurring within halos from large-scale evolution and mitigating assembly bias.

[ARZ: Put a discussion of Fig. 15 here. It does not need to reiterate the discussion of Fig. 14. However, it should state that we reach the same broad conclusion and that this is good in part because c_V is a nonparametric measure of halo concentration.] Figure 15 follows the same exercise as above, with a comparison drawn to the Fig. 9. Notice that the same trends as Fig. 14 can be seen: a significant fraction of assembly bias is removed as compared to the unmatched catalog, though statistically significant assembly bias remains. Only in combination with halo redefinition do we remove assembly more completely on large scales. Note that the max circular velocity defined concentration is nonparametric by design; this helps to confirm that our result is not related to choice of halo density profile.

[ARZ: This paragraph is good, but needs to be written a bit more professionally. Start with a sentence like, "It is interesting to explore the reasons that halo shape, spin, and satellite number are not amenable to having their assembly bias mitigated through simple halo redefinitions." Then move on to some specifics.] **[ASV: attempted to rewrite more professionally!]**

While halo shape, spin, and satellite number are not amenable to having their assembly bias mitigated through the simple halo redefinition technique we have suggested, the underlying reasons for this behavior remains of interest for exploration. In the case of halo shape, we suggest that the assembly bias may be driven through interactions with large scale structure. Studies have shown a statistically significant alignment between filaments and satellite galaxy position (Tempel et al. 2015; Velliscig et al. 2015)**[ASV: need to grab paper from arxiv 2016.05.09 for this]**.

Note that the mass dependence of assembly bias is implicitly explored with our suite of simulations. The nature of the MCFs emphasizes halos just above the threshold mass; e.g. L0125 probes the smallest mass halos, while L0250 probes the largest mass halos. To more explicitly explore this mass dependence, Figure 16 demonstrates how bias scales as a function of both fixed halo mass and choice of overdensity Δ. Here we calculate the bias as follows:

$$b^2(r) = \xi_{c_{\rm NFW}}/\xi_{\rm all}, \tag{9}$$

where $\xi_{c_{\rm NFW}}$ consists of those halos with the 20% highest marks in NFW-defined concentration and $\xi_{\rm all}$ consists of all halos. Note that due to the limited number of halos in each mass bin, we choose not to use the binning and rank weighting that is utilized in previous analysis. **[ASV: This is currently how it is run and I am not sure if this is the best approach. We could probably afford to use 5 bins and it would be a little more fine than when we carry out the full analysis.]** To explore the mass dependency of the bias, we choose to examine a fixed scale of 5 to 10 h^{-1}Mpc . We calculate the bias using halos in bins of fixed mass, with errors calculated using resampling in which $\xi_{\rm all}$ is replaced with the correlation function calculated using a randomly chosen subsample of equal number to the biased subsample. The displayed error bars represent the region in which 68% of these random subsamples lie. We explore our

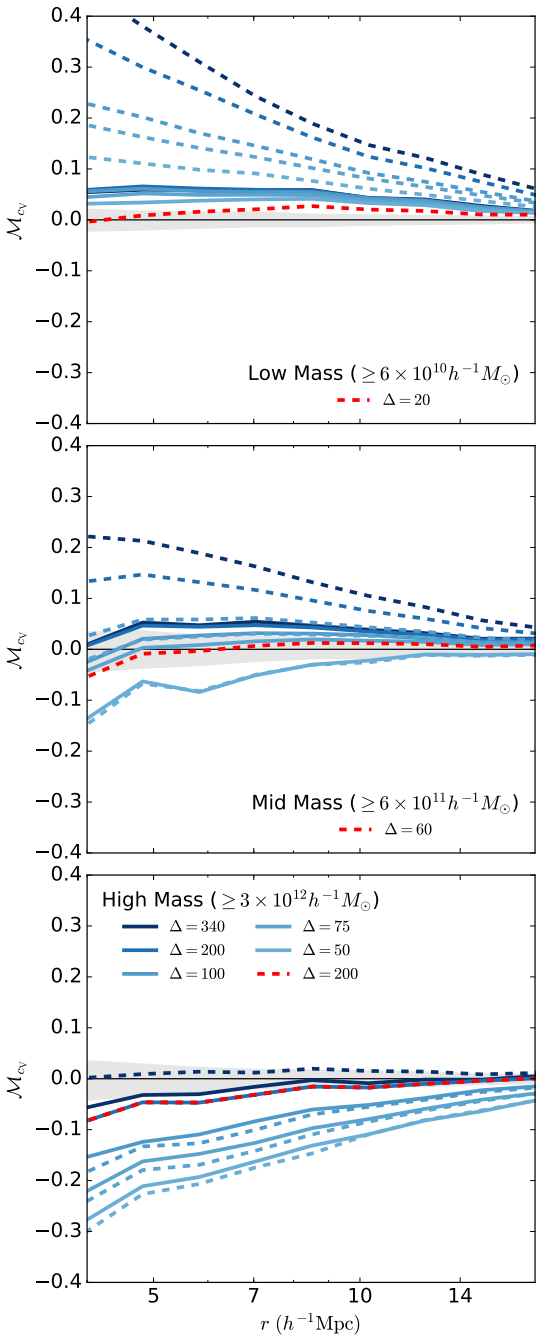

Figure 15. The marked correlation function for the velocity ratio defined halo concentration parameter. The solid lines plot the marked correlation function using velocity ratio halo concentration as the mark, for a catalog matched against the best fit Δ shown in red. The dashed lines plot the original marked correlation function results. In each plot the lines correspond to different values of Δ, with dark blue (light blue) corresponding to $\Delta = 340$ ($\Delta = 50$). The red dashed line corresponds to the overdensity chosen for matching as possibly removing assembly bias on most scales for halo concentration. The top (middle/bottom) panel shows the results for the L0125 (L0250/L0500) data set utilizing the low mass (mid mass/high mass) cutoffs. The shaded bands represent 2-sigma confidence regions generated by randomization of the marks.

dataset with the following binning, in which the larger simulations are able to push to higher masses than the smallest simulation: $7\times10^{10}-2\times10^{10}, 2\times10^{10}-7\times10^{11}, 7\times10^{11}-2\times10^{12}, 2\times10^{12}-7\times10^{12}, 7\times10^{12}-2\times10^{13}, 2\times10^{13}-7\times10^{13}, 7\times10^{13}-2\times10^{14}\ h^{-1}\mathrm{M}_{\odot}$.

There are two clear trends to be determined from this data. The first is the trend for the assembly bias with halo concentration to be reduced as a function of halo mass. This trend helps to resolve the apparent inconsistencies in measures of assembly bias in the literature; namely, a change in halo mass of interest can lead to a considerably different measure of halo assembly bias - at high masses, halo assembly bias due to NFW-defined concentration is fairly minimal. The second visible trend is that a change in halo definition chosen has a trend of decreasing the halo bias determined. Furthermore, it should be noted that this can lead to an anticlustering of halos of high concentration at high masses. These two discoveries seem to suggest that halo assembly bias of NFW-defined halo concentration is a coincidence; choosing a halo size across all halo masses as a function of an overdensity will be insufficient in creating self-similiar dark matter halos. **[ARZ: Instead, add one summarizing paragraph here discussing the mass dependence of assembly bias. Emphasize that our findings suggest that the strength of assembly bias can be a strong function of halo definition and that this may already be making it difficult to compare the results of various different research groups using different halo definitions.]**

7 CONCLUSIONS

[ARZ: After dealing with the comments above, let's come back to rewriting the conclusions section.] We have looked at how to use CFs and MCFs in order to analyze the environmental effects upon the properties of the halo. We have suggested a method of removing the mass dependence that is not subject to the small number statistics at large halo masses. Taking our various tests, we then apply a change to the threshold density Δ in an attempt to remove the effect that environment has upon these properties. We come to the following conclusions from our simulation data.

- Our halo redefinition method does not cause any substantial breakdown in the ROCKSTAR halo finding algorithm, though this may not be the case for every halo finding methodology. This is something that should be considered prior to utilization of this method, unless working directly from particle data. As our initial halo sizes and locations are determined through spherical overdensities, it cannot be assumed that starting from a FoF grouping and then determining values through particle data directly will produce identical results. Similarly, different cosmologies may remove environmental effects at different scales.
- When looking at the two-point correlation function, there appears to be a "sweet spot" that appears to remove environmental effects the most efficiently. Going beyond that seems to reintroduce environmental effects, possibly as an extreme side effect of halo exclusion.
- For our marked correlation functions we see that both proxies of concentration that we use as marks show significant removal of environmental effects at large scales for similar values of the overdensity parameter Δ. In cases where one is only interested in the concentration of dark matter halos and large scales (or correspondingly small values of k), this method will allow you to compensate for bias that environment could introduce to calculations dependent upon the halo model. This may prove valuable for calculations such as that of the shear power spectrum calculated through weak lensing.
- The environmental effects on the shape of the host halo and the satellite number of the host halo cannot be removed regardless of the chosen redefinition of Δ. We propose that this may be intrinsically tied to the nature of the filaments, whose effects cannot be removed by a simple redefinition of the halo radius.
- This method is definitively related to the mass of the halos that are being observed. Furthermore, it appears that the majority of the reduction in assembly bias is tied to the exclusion of halos from the catalog as a result of being subsumed into larger halos. This information does not seem to be contradictory; it can be intuitively understood that the region about the most massive halos will be different than the region around the least massive halos, leading to a different frequency at which halos are being excluded. It does however warrant that careful consideration be given to the sample of halos that are of interest.
- The selection of halo size is intrinsically related to the assembly bias and varies across scales. This might help to resolve contradictory results in the search for halo assembly bias in the literature.

This methodology, while certainly not perfect in accounting for assembly bias, may be of significance when applied to galaxy formation models and give insight into seemingly conflicting results. Provided that the properties of interest in a given model behave well under our redefinition, it will allow us to create better mock galaxy catalogs without resorting to more complicated models requiring halo formation histories - giving us another powerful tool to test observation against.

There remain possible uncertainties to study in the future. One possible area of follow-up is the matter of simulation cosmology, which is not explored in this text. It is possible that the choice of cosmology may change observed assembly bias as a function of the halo masses, something that our methodology should be capable of observing. Furthermore, we can determine if the choice of halo size that best reduces assembly bias is a function of the chosen cosmology. This may be of interest in attempting to determine signatures of assembly bias in observational samples in the future.

ACKNOWLEDGMENTS

We are grateful to many people. Our calculations are carried out utilizing the `numpy` (Walt et al. 2011), `astropy` (Astropy Collaboration et al. 2013), `matplotlib` (Hunter 2007), and `halotools` (Hearin et al. 2016a) packages in Python.

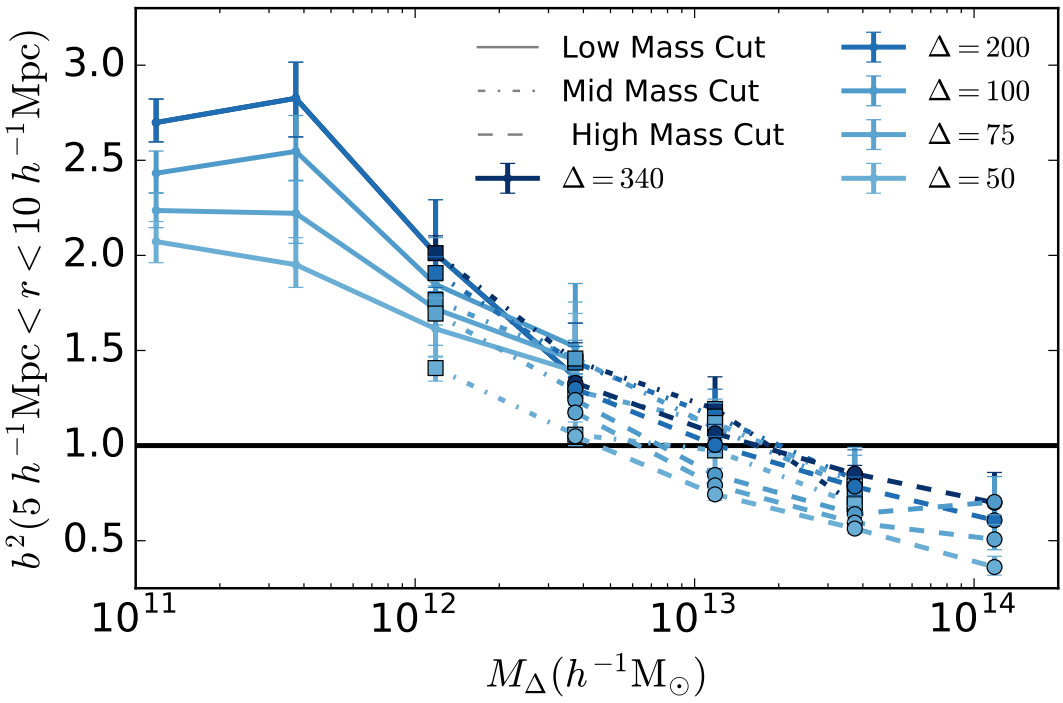

Figure 16. The bias of the 20% highest concentration sample to the full sample, plotted against halo mass measured at the halo radius. The halo mass binning is defined in full detail in the text. Halo definitions descend from the largest definition to lowest definition, from dark to light in color. The dark blue (light blue) line uses a halo definition drawn from $\Delta = 340$ ($\Delta = 50$). The solid (dot-dashed, dashed) lines use host halos from the L0125(L0250,L0500) catalogs. The error bars encompass 68% of measurements using two hundred subsamples of the mark of the same size as the biased sample. The solid black line shows where there is no detected assembly bias driven by NFW-defined halo concentration.

REFERENCES

Adhikari S., Dalal N., Chamberlain R. T., 2014, J. Cosm. Astropart. Phys., 11, 019

Allgood B., Flores R. A., Primack J. R., Kravtsov A. V., Wechsler R. H., Faltenbacher A., Bullock J. S., 2006, MNRAS , 367, 1781

Astropy Collaboration et al., 2013, Astron. & Astrophys. , 558, A33

Behroozi P. S., Wechsler R. H., Wu H.-Y., 2013a, Astrophys. J. , 762, 109

Behroozi P. S., Wechsler R. H., Conroy C., 2013b, Astrophys. J. , 770, 57

Bett P., Eke V., Frenk C. S., Jenkins A., Helly J., Navarro J., 2007, MNRAS , 376, 215

Blumenthal G. R., Faber S. M., Primack J. R., Rees M. J., 1984, Nature , 311, 517

Bullock J. S., Wechsler R. H., Somerville R. S., 2002, MNRAS , 329, 246

Cacciato M., van den Bosch F. C., More S., Mo H., Yang X., 2013, MNRAS , 430, 767

Chaves-Montero J., Angulo R. E., Schaye J., Schaller M., Crain R. A., Furlong M., Theuns T., 2016, MNRAS , 460, 3100

Conroy C., Wechsler R. H., 2009, Astrophys. J. , 696, 620

Croton D. J., Gao L., White S. D. M., 2007, MNRAS , 374, 1303

Dalal N., White M., Bond J. R., Shirokov A., 2008, Astrophys. J. , 687, 12

Despali G., Giocoli C., Bonamigo M., Limousin M., Tormen G., 2016, preprint, (arXiv:1605.04319)

Diemer B., Kravtsov A. V., 2014, Astrophys. J. , 789, 1

Diemer B., Kravtsov A. V., 2015, Astrophys. J. , 799, 108

Duffy A. R., Schaye J., Kay S. T., Dalla Vecchia C., 2008, MNRAS , 390, L64

Faltenbacher A., White S. D. M., 2010, Astrophys. J. , 708, 469

Fisher J. D., Faltenbacher A., 2016, preprint, (arXiv:1603.06955)

Gao L., White S. D. M., 2007, MNRAS , 377, L5

Gao L., White S. D. M., Jenkins A., Frenk C. S., Springel V., 2005, MNRAS , 363, 379

Gil-Marín H., Jimenez R., Verde L., 2011, MNRAS , 414, 1207

Guo Q., et al., 2011, MNRAS , 413, 101

Guo H., et al., 2014, MNRAS , 441, 2398

Hahn O., Porciani C., Carollo C. M., Dekel A., 2007a, MNRAS , 375, 489

Hahn O., Carollo C. M., Porciani C., Dekel A., 2007b, MNRAS , 381, 41

Harker G., Cole S., Helly J., Frenk C., Jenkins A., 2006, MNRAS , 367, 1039

Hearin A., et al., 2016a, preprint, (arXiv:1606.04106)

Hearin A. P., Zentner A. R., van den Bosch F. C., Campbell D., Tollerud E., 2016b, MNRAS , 460, 2552

Hunter J. D., 2007, Computing In Science & Engineering, 9, 90

Kazantzidis S., Zentner A. R., Kravtsov A. V., 2006, Astrophys. J. , 641, 647

Lacerna I., Padilla N., 2011, MNRAS , 412, 1283

Leauthaud A., et al., 2012, Astrophys. J. , 744, 159

Li Y., Mo H. J., Gao L., 2008, MNRAS , 389, 1419

Mao Y.-Y., Williamson M., Wechsler R. H., 2015, Astrophys. J. , 810, 21

Mo H., van den Bosch F. C., White S., 2010, Galaxy Formation and Evolution

More S., van den Bosch F. C., Cacciato M., More A., Mo H., Yang X., 2013, MNRAS , 430, 747

More S., Diemer B., Kravtsov A. V., 2015, Astrophys. J. , 810,

36
Moster B. P., Naab T., White S. D. M., 2013, MNRAS , 428, 3121
Navarro J. F., Frenk C. S., White S. D. M., 1997, Astrophys. J. , 490, 493
Peacock J. A., Smith R. E., 2000, MNRAS , 318, 1144
Peebles P. J. E., 1969, Astrophys. J. , 155, 393
Porciani C., Norberg P., 2006, MNRAS , 371, 1824
Rodríguez-Puebla A., Drory N., Avila-Reese V., 2012, Astrophys. J. , 756, 2
Sheth R. K., 2005, MNRAS , 364, 796
Sheth R. K., Tormen G., 2004, MNRAS , 350, 1385
Sunayama T., Hearin A. P., Padmanabhan N., Leauthaud A., 2016, MNRAS , 458, 1510
Tempel E., Guo Q., Kipper R., Libeskind N. I., 2015, preprint, (arXiv:1502.02046)
Tinker J. L., Weinberg D. H., Zheng Z., Zehavi I., 2005, Astrophys. J. , 631, 41
Tinker J. L., Leauthaud A., Bundy K., George M. R., Behroozi P., Massey R., Rhodes J., Wechsler R. H., 2013, Astrophys. J. , 778, 93
Valluri M., Vass I. M., Kazantzidis S., Kravtsov A. V., Bohn C. L., 2007, Astrophys. J. , 658, 731
Velliscig M., et al., 2015, preprint, (arXiv:1504.04025)
Wake D. A., et al., 2011, Astrophys. J. , 728, 46
Walt S. v. d., Colbert S. C., Varoquaux G., 2011, Computing in Science and Engg., 13, 22
Wang H. Y., Mo H. J., Jing Y. P., 2007, MNRAS , 375, 633
Warnick K., Knebe A., Power C., 2008, MNRAS , 385, 1859
Wechsler R. H., Bullock J. S., Primack J. R., Kravtsov A. V., Dekel A., 2002, Astrophys. J. , 568, 52
Wechsler R. H., Zentner A. R., Bullock J. S., Kravtsov A. V., Allgood B., 2006, Astrophys. J. , 652, 71
Wetzel A. R., Nagai D., 2015, Astrophys. J. , 808, 40
Wetzel A. R., Tinker J. L., Conroy C., van den Bosch F. C., 2014, MNRAS , 439, 2687
White S. D. M., Rees M. J., 1978, MNRAS , 183, 341
Yang X., Mo H. J., van den Bosch F. C., 2003, MNRAS , 339, 1057
Yang X., Mo H. J., van den Bosch F. C., 2009, Astrophys. J. , 695, 900
Yang X., Mo H. J., Zhang Y., van den Bosch F. C., 2011, Astrophys. J. , 741, 13
Yang X., Mo H. J., van den Bosch F. C., Zhang Y., Han J., 2012, Astrophys. J. , 752, 41
Zehavi I., et al., 2005, Astrophys. J. , 630, 1
Zehavi I., et al., 2011, Astrophys. J. , 736, 59
Zentner A. R., 2007, International Journal of Modern Physics D, 16, 763
Zentner A. R., Berlind A. A., Bullock J. S., Kravtsov A. V., Wechsler R. H., 2005, Astrophys. J. , 624, 505
Zentner A. R., Hearin A. P., van den Bosch F. C., 2014, MNRAS , 443, 3044
Zhao D. H., Mo H. J., Jing Y. P., Börner G., 2003, MNRAS , 339, 12
Zhao D. H., Jing Y. P., Mo H. J., Börner G., 2009, Astrophys. J. , 707, 354
Zheng Z., Coil A. L., Zehavi I., 2007, Astrophys. J. , 667, 760
Zu Y., Mandelbaum R., 2015, MNRAS , 454, 1161
van Daalen M. P., Angulo R. E., White S. D. M., 2012, MNRAS , 424, 2954
van den Bosch F. C., et al., 2007, MNRAS , 376, 841

APPENDIX

One natural question that might arise in the analysis of this work is the nature of the resulting assembly bias trends. Our focus in the main sections of this paper is on the nature of the assembly bias changing as a function of the mass cut chosen. Our conclusions include the fact that there is a strong mass dependence on halo assembly bias that must be accounted for separately depending on the halos of interest in a study. However, while the existence of this trend is clear within our analysis, the determination that this is solely due to the masses of the halos included in our calculation is less clear upon closer inspection. One possibility that might be particularly concerning is the potential that the different simulations have created halos that have fundamentally different clustering and this is leading to the result that we are interpreting as a mass dependence on assembly bias. Thankfully, though our statistics become less meaningful to carry out this calculation, we can carry out a comparison using the same mass cut across two of our simulations, knowing that these will only contain well resolved halos.

While not addressed directly, Figure **??** through Figure **??** contain a demonstration of the result that we are seeking in the left column of panels. The lower left panels show various marks of interest for L0250 using the "mid mass" cut on the data set. In comparison, the upper left panel contains the same marks of interest for the L0125 using the same mass cut. In the latter, there are fewer halos in this mass cut range, as a result of the smaller simulation box size. However, we note that despite the additional noise in the data set, the behavior of the assembly bias measurement is nearly identical within tolerances accounting for differences between simulations and noise. This motivates our conclusion that the driver behind the behavior is the mass cut of the data sets rather than the resolution of the simulation.